電弱スケールにおける複数段階相転移

著者	澁谷 紘人
著者別表示	SHIBUYA Hiroto
雑誌名	博士論文要旨Abstract
学位授与番号	13301甲第5680号
学位名	博士（理学）
学位授与年月日	2023-03-22
URL	http://hdl.handle.net/2297/00069891

Dissertation Abstract

電弱スケールにおける複数段階相転移

Multi-step electroweak phase transition

Division: Mathematical and Physical Sciences
Name: Hiroto Shibuya

Abstract

The electroweak phase transition (EWPT), which occurs at a temperature around 100 GeV in the universe and gives the particle masses, can be footholds of the progresses in particle physics. In the dissertation, we mainly studied the multi-step PTs, which mean the PT occurs multiple times and have gotten attention recently. First, we studied their features and revealed the causes. Furthermore, as physical signatures of the multi-step PTs, we predicted the deviation of the Higgs trilinear coupling from that in the standard model and the multi-peaked GW spectrum yield by the first-order PTs. Next, we discussed the impacts of the PTs on dark matter production. We used the scotogenic model as a benchmark model and revealed it could be consistent with current experiments by considering the PT effects, while it does not match the experiments in the conventional calculation. The model can also explain the neutrino masses, which are absent in the standard model. Lastly, we studied the baryon number asymmetry produced by the multi-step PTs using a simplified scenario. We showed that adequate asymmetry could be reproduced via the multi-step. Specific models for the scenario are also discussed, and we showed the concrete PTs which could allow enough asymmetry.

Particle physics considers four types of interactions among particles, i.e., gravity, strong, weak, and electromagnetic interactions. Gravity is much weaker than the other interactions in calculations of particle physics. Hence, the standard model (SM) in particle physics includes three interactions except for gravity. The weak and electromagnetic interactions can be written uniformly, while we can treat the strong interaction independently from the two interactions. In this dissertation, we discuss the electroweak (EW) theory mainly.

The SM explains various experiments very well. However, there are some significant problems:

- asymmetry between particles and anti-particles,
- existence of dark matters (DMs),
- neutrino masses.

The first problem indicates the question, why only particles remain in the universe and the anti-particles not? An observed number of baryons, which are consisted of three elementary particles like protons and neutrons, is $(n_B - n_{\bar{B}})/n_\gamma \sim 10^{-10}$ [1]. The indexes $n_B, n_{\bar{B}}$, and n_γ represent the number density of baryons, anti-baryons, and photons. SM cannot explain this baryon number asymmetry in the universe (BAU). Hence, some new mechanisms are needed. The second problem is the existence of the DMs, which are proved by the observations of cosmic micro background (CMB), gravitational lens, and so on. They consist of about 85% of matter in the universe and about 27% of the global energy budget [2]. It is still unknown what the DM is, whereas many candidates are proposed. The last problem we mentioned is the neutrino masses. The existence of neutrinos was proved in the 1950s by Ref. [3]. Super-Kamiokande, which was a developed version of the Kamiokande, found the neutrino oscillation [4]. That indicates the existence of neutrino masses, which are ignored in the SM. Therefore, we need some new mechanisms giving the masses.

The reasons why the SM cannot explain the BAU are as follows. To yield the BAU, a theory needs to satisfy Sakharov's three conditions [5]:

- baryon number violation,
- C and CP violations,
- departure from equilibrium.

Baryon number violation means the number difference of the baryons and anti-baryons occurred in interactions. Without this violation, the number of the baryons cannot exceed that of the anti-baryons. C and CP violations represent asymmetries between particles and anti-particles, which are also needed for the BAU. If the last condition, the departure from equilibrium, is not satisfied, the BAU cannot be accomplished because an inverse baryon number violation process occurs, and the number violation vanishes. In the SM, the conditions, except for the first, are not satisfied enough. Although the SM contains the CP violation (CPV) called Cabbibo-Kobayashi-Maskawa phase [6], the violation is too small to realize the observed BAU. Therefore, some new CPV sources are needed. To accomplish the departure from the equilibrium, an EW phase transition (PT) has to be the first-order. The EWPT is considered to occur at a temperature of around 100 GeV in the universe. After the PT, particles in the SM acquire their masses. Higgs particle, which was found in 2012 in the LHC [7, 8], would be the proof of this mechanism giving the particle masses. The PT occurs via the temperature change of the scalar potential and the acquisition of the vacuum expectation value (VEV) of the scalar field. It becomes the first-order when the potential barrier arises between two minima and tunneling occurs to the deeper one. When the first-order PT occurs in the universe, bubbles appear in the universe as same with boiling water. It is known that the PT in the SM is not the first-order, but the smooth PT called cross-over [9]. From above, the SM cannot explain the BAU.

The BAU can be explained by extending the scalar sector of the SM, which gives particle masses. The sector is given in the simplest form. Hence, there are possibilities for the extension. One example is the two Higgs double models (2HDMs). It simply adds one more $SU(2)_L$ scalar doublet to the SM. The 2HDM contains the minimal supersymmetric standard model as

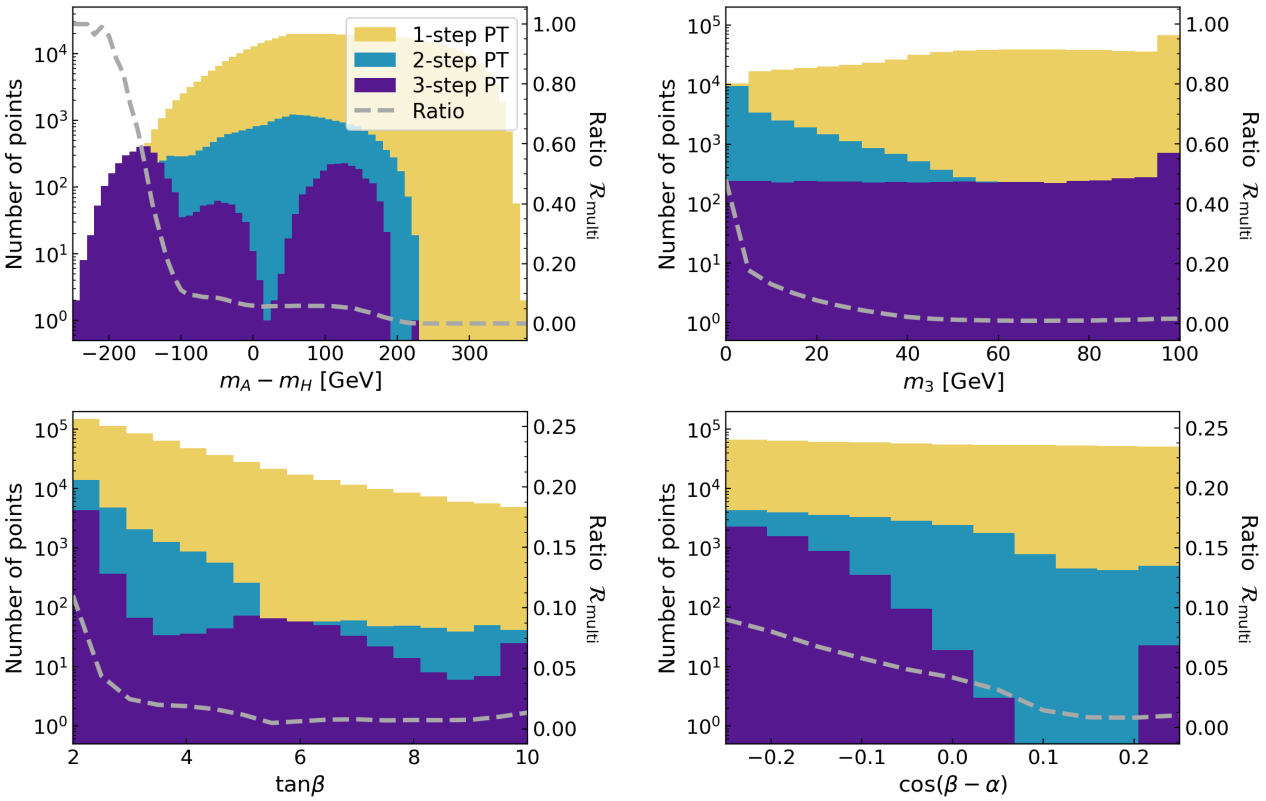

Figure 1 Number of points where the 1-step and multi-step PTs occur as a function of $m_A - m_H$ (upper left), m_3 (upper right) $\tan\beta$ (lower left) and $\cos(\beta-\alpha)$ (lower right). The 1-step, 2-step, and 3 or more step PTs are colored yellow, blue, and purple, respectively. The grey dashed lines in the panels represent $\mathcal{R}_{\rm multi}$, which are the ratios of the number of points for the multi-step PTs to that for all PTs and denotes how likely to occur the multi-steps.

a subset. Supersymmetric theories have a possibility to be higher energy scale theories than the EW theories. Hence, research on 2HDMs could be footholds for them. The 2HDMs can satisfy the Sakharov conditions. They can contain new CPV sources in the scalar sector, and the PT can be first-order. Because they have multiple physical scalar fields, the EWPT can occur multiple times. We call such PTs as *multi-step PTs*. Although they were proposed in, e.g., Ref. [10], their features have not been studied in great detail. In this dissertation, we revealed their features in the CP-conserving 2HDMs by performing larger-scale parameter searches [11] than the previous studies for the usual one-step PT [12]. As a result, we found the features of the multi-step PTs as

- large non-decoupling effect,
- large contribution of a scalar potential parameter, which makes PTs into multi-step,
- the approximate discrete symmetry in the scalar potential.

To describe these features, we show the number of points where the 1-step and multi-step PTs occur in the Type-I 2HDM with $m_A = m_{H^\pm}$ as a function of $m_A - m_H$ (upper left), m_3 (upper right) $\tan\beta$ (lower left) and $\cos(\beta-\alpha)$ (lower right) in Fig. 1. The indexes $m_{H^\pm}, m_A$, and m_H represent masses of the exotic charged, neutral CP-odd and CP-even scalar fields, m_3 is the soft Z_2 breaking parameter in the scalar potential, and α and β are the mixing angles for diagonalizing scalar mass matrixes. The 1-step, 2-step, and 3 or more step PTs are colored yellow, blue, and purple, respectively. The grey dashed lines in the panels represent $\mathcal{R}_{\rm multi}$, which are the ratios of the number of points for the multi-step PTs to that for all PTs and denotes how likely to occur the multi-steps. From the figure, we can see that the multi-step PTs favor the largeness

of $|m_A - m_H|$, small m_3, $\tan\beta$, and $\cos(\beta-\alpha)$. The first and second parameter features, which correspond to the upper panels in Fig. 1, indicate the large non-decoupling effects in the scalar sector. The effects make differences in some observable between the SM and 2HDMs. Hence, the multi-step PTs favor the large differences from the SM. The last two parameter features, which are related to the lower panels in Fig. 1, represent the largeness of the scalar potential parameter which makes PTs into multi-step PTs. The scalar potential in the 2HDMs we considered has eight parameters. We found that one parameter in the potential plays an important role in inducing multi-step PTs. We also revealed small $\tan\beta$ and $\cos(\beta-\alpha)$ are associated with the significant contribution from the potential parameter. The last feature, the approximate discrete symmetry in the scalar potential, is related to small m_3 because m_3 breaks the symmetry in the potential.

As physical signatures of the multi-step PTs, we studied the deviations $\delta\lambda_{hhh}$ of the Higgs trilinear coupling from that in the SM. The left panel of Fig. 2 shows $\delta\lambda_{hhh}$ predictions for the 1-step, 2-step, and 3 or more step PTs in the Type-I 2HDM with $m_A = m_{H^\pm}$. We can see the parameter points where the multi-step PTs happen are located on the upper side of the plots in the region $m_A \gtrsim 300$ GeV. In other words, compared with the results of the 1-step PTs, the values of $\delta\lambda_{hhh}$ for the multi-step PTs have a tendency to be large at the same value of m_A. At the future measurement, like the HL-LHC, limits on the Higgs trilinear coupling could reach an accuracy of about 50–60% with 3 ab^{-1} data [13], while the ILC operating at 500 GeV has the possibility to measure $\delta\lambda_{hhh}$ with 27% of precision [14]. Hence, the signature of the multi-step PTs in the collider experiments could be found. We also predicted the multi-peaked gravitational wave (GW) from the multi-step PT. The first-order PT yields the GW spectrum, so if it occurs multiple times, the multi-peaked GW spectrum can be observed. The right panel of Fig. 2 shows the spectrum $h^2\Omega_{\text{GW}}$ from the 2-step PT at a certain parameter set. The observable areas by the future space-based interferometers such as LISA [15], DECIGO [16], BBO [17], U-DECIGO [18], Taiji [19], and TianQin [20] are also presented by colored regions. The navy and blue lines represent the GW spectrums from the first and second step PTs, which have peak frequencies around 0.1 Hz and 2×10^{-3} Hz, respectively. The superposed GW spectrum is shown by the red line. We can see that it has a double peak, which can be observed by BBO or U-DECIGO. Additionally, the deviation of the Higgs trilinear coupling $\delta\lambda_{hhh}$ is obtained as 2.2 with the multi-peaked spectrum. Such $\delta\lambda_{hhh}$ has the possibility to be measured at the HL-LHC and the ILC. Therefore with a combination of the signatures from colliders and GW interferometers, it might be possible to identify whether the multi-step PT occurred in the early universe.

In the different model from above, but containing the 2HDM, we also studied the impacts of the first-order PTs on DM production [21]. The model is called the scotogenic model, which is one of the economical models accommodating the small neutrino masses and DM in the universe simultaneously [22]. However, it is non-consistent with current experiments. We consider the two types of PTs, which are 1-step and 2-step PTs, shown in Fig. 3. In the dissertation, we took some benchmark parameter sets to demonstrate the impacts of the PTs. Fig. 4 shows example solutions of the coupled Boltzmann equations (top), the scalar masses with thermal effects (middle), and the reaction rates (bottom) for the one-step PT where the dark matter mass and the Yukawa coupling are fixed at $(m_N,\ |\mathbb{Y}|) = (710\text{ GeV},\ 1.00 \times 10^{-5})$ for the left panels, and $(870\text{ GeV},\ 1.54 \times 10^{-7})$ for the right panels, respectively. The vertical red lines indicate when the first-order PT occurs. The left (right) panels represent the results where the DM candidate right-handed (RH) neutrino N is (not) thermalized from the beginning. In both cases, the DM abundances are fixed instantly at the PT and match with the observed values shown by horizontal black dotted lines. The abundance in the left panel is determined by the thermal DM number density n_N^{eq}, hence the RH neutrino mass m_N in n_N^{eq} decides it if the transition temperature is fixed. By contrast, the Yukawa coupling $|\mathbb{Y}|$ determines the abundance in the right panels. To influence the abundance, the transition temperature T_n is needed to

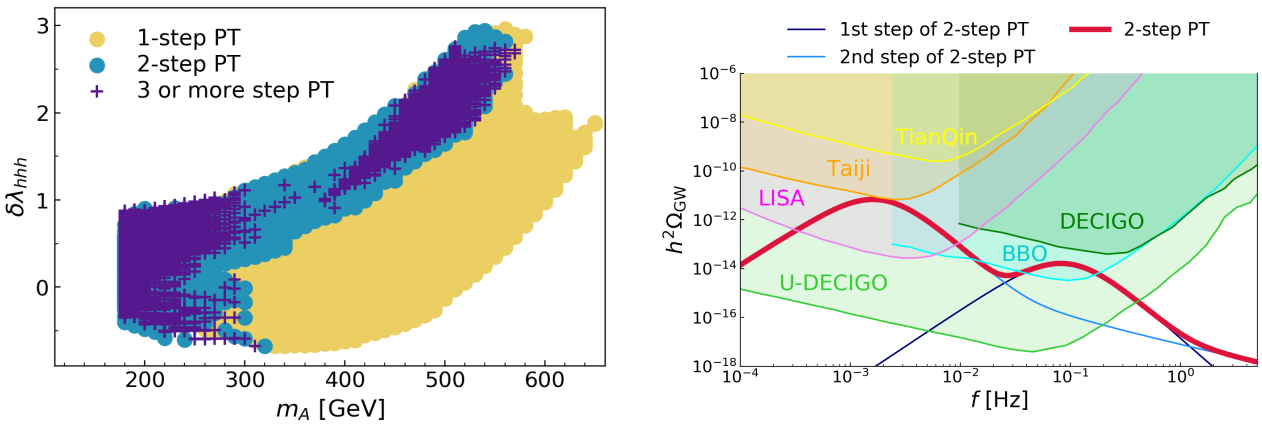

Figure 2 Left: Predictions for $\delta\lambda_{hhh}$ in the Type-I 2HDM with $m_A = m_{H^\pm}$. The panels except for the lower right panel show $\delta\lambda_{hhh}$ where the 1-step, 2-step, and 3 or more step PTs occur for m_A. Right: GW spectrums from the first and second step of the strong 2-step PT for the benchmark point. The navy and blue lines represent the GW spectrums from the first and second step PTs, respectively. The red line shows the superposed GW spectrum.

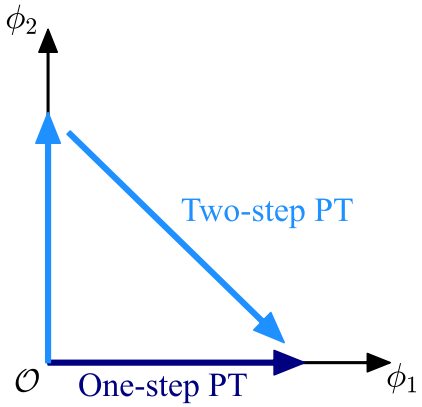

Figure 3 Schematic picture of one-step and two-step PTs.

satisfy $m_N/T_n \geq 20$. Note that if we do not consider the effects of the PT, the DM abundance becomes much larger than the observed value. Next, Fig. 5 shows example solutions for the Boltzmann equation with the two-step PTs (left) and the masses of the inert scalars and gauge bosons with thermal effects (right). The dark matter mass and the Yukawa coupling are fixed at $(m_N,\ |\mathbb{Y}|) = (1\ \text{GeV},\ 2.1 \times 10^{-12})$ for the left panels and $(10\ \text{GeV},\ 2.8 \times 10^{-12})$ for the right panels. The two-step case does not satisfy the condition for influencing the freeze-out mechanism, hence we consider the freeze-in mechanism. We can see that the PT makes the abundance much larger than that without the effect. In this case, the duration of m_N/T between the first and second PTs is important. Therefore, the condition for affecting the abundance requires a longness of duration. For the physical signature of our scenarios, we calculated the GW spectrums from the first-order PTs. Fig. 6 shows peaks of the GW energy density fraction as a function of the frequency for the one-step* PT (red) and the 2nd PT of the two-step* (blue). The colored regions are observable areas by future space-based interferometers. The conditions for impacting the DM abundance acquire the low transition temperatures. Hence, the significant latent heat, which makes the energy density of the GW spectrums larger, would be generated via the first-order PTs. In fact, we can see that the large part of the spectrums in Fig. 6 can be observed by the future interferometers. Especially the red point for the one-step scenario can be clarified by LISA. Such unusual behaviors happen because the conditions restrict the transition temperature.

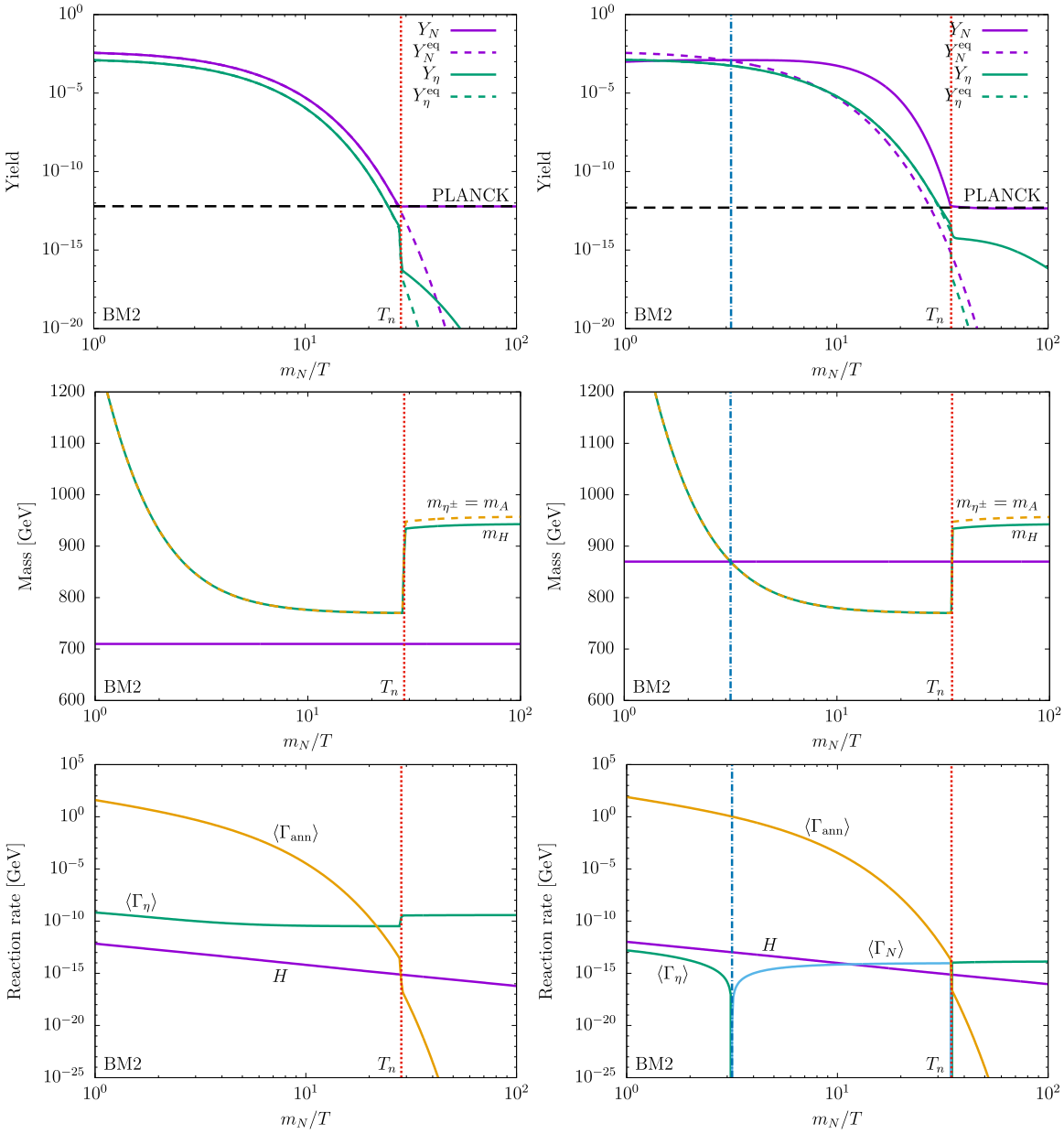

Figure 4 Example solutions of the coupled Boltzmann equations (top), the scalar masses with thermal effects (middle), and the reaction rates (bottom) for the one-step PT where the dark matter mass and the Yukawa coupling are fixed at $(m_N,\ |\mathbb{Y}|) = (710\ \text{GeV},\ 1.00\times10^{-5})$ for the left panels, and $(870\ \text{GeV},\ 1.54\times10^{-7})$ for the right panels, respectively.

In conclusion, by considering the impacts of the PTs, the calculation of the DM abundance could be changed. In particular, the scotogenic model can be consistent with current experiments by the effects of the PTs. The GW interferometers can clarify the scenarios.

Lastly, we studied the realization observed BAU via the multi-step PTs. To describe the EW baryogenesis (BG), we consider a simplified scenario as shown in Fig. 7. We studied the BG via the top transport, hence the complex top mass m_t induces the CP violation and makes the BAU. We define it as $m_t \propto (\phi + i\phi_{CP})$. The indexes ϕ and ϕ_{CP} indicate the neutral CP-even and CP-odd scalar field values. At the first step of the PT, only ϕ_{CP} gets the VEV as in Fig. 7. The BAU is produced via the second step, which is the first-order, because of the change of the complex phase for the top mass. A benchmark second PT is shown in the right panel of Fig. 7. The horizontal axis z indicates the coordinate along the bubble radius, while the bubble

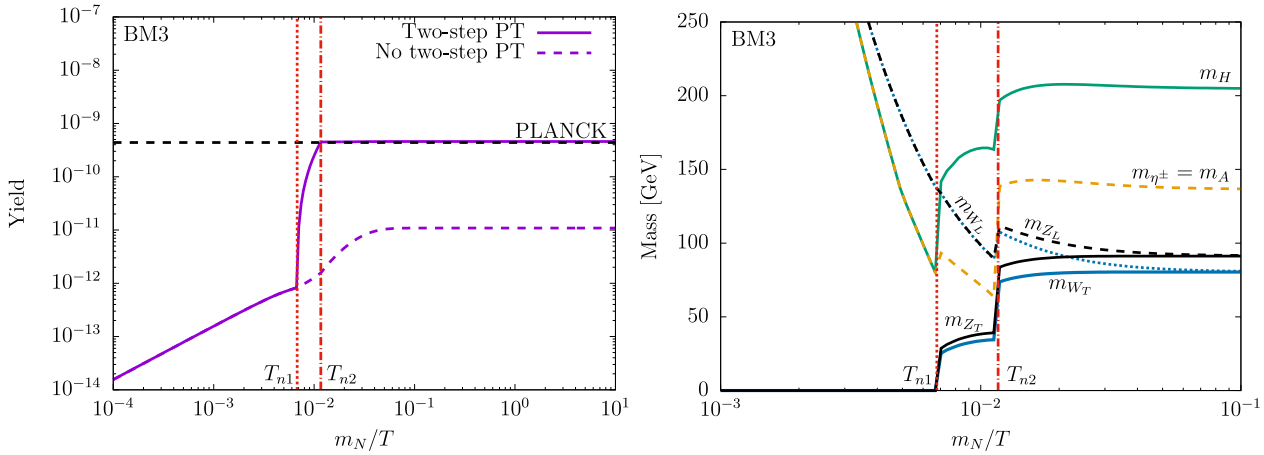

Figure 5 Example solutions for the Boltzmann equation with the two-step PTs (left) and the masses of the inert scalars and gauge bosons with thermal effects (right). The dark matter mass and the Yukawa coupling are fixed at $(m_N,\ |\mathbb{Y}|) = (1\ \text{GeV},\ 2.1 \times 10^{-12})$ for the left panels and $(10\ \text{GeV},\ 2.8 \times 10^{-12})$ for the right panels.

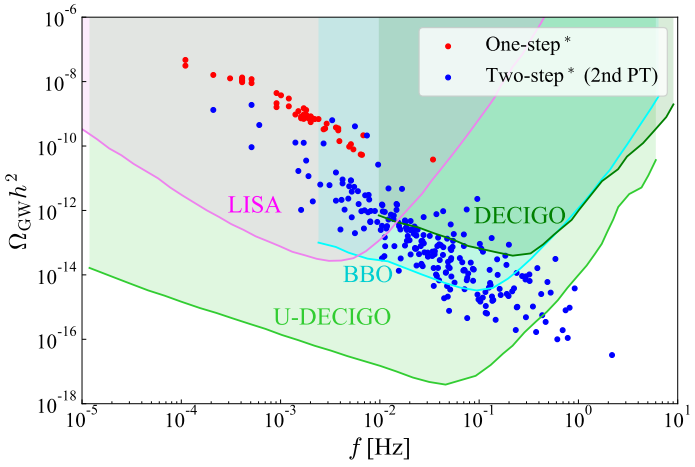

Figure 6 Peaks of the GW energy density fraction as a function of the frequency for the one-step* PT (red) and the 2nd PT of the two-step* (blue). The colored regions are observable areas by future space-based interferometers.

wall locates at $z = 0$. The left panel of Fig. 8 represents sphaleron rates $\Gamma_{\rm sph}/T$ as the function of ϕ/T. The sphaleron process is needed to satisfy Sakharov's first condition, baryon number violation. The largeness of its rate $\Gamma_{\rm sph}$ influences the amount of the produced BAU. In the left panel of Fig. 8, we represent the rate in various cases. The blue line shows the rate in symmetric phase $(\phi, \phi_{CP}) = (0, 0)$, the green line indicates that in the broken phase with the parameter $\kappa = 0.1$, and the orange line shows that via the CKT prescription proposed in Ref. [23]. We can see the green line exceeds the blue line in $0.1 \lesssim \phi/T \lesssim 0.4$. Ref. [24] insults this behavior would come from the breakdown of the approximation, which is used to derive the sphaleron rates in the broken phase. To obtain the precise result, we need to use the non-perturbative calculation via lattice calculation. In this dissertation, we try to use the rate with $\kappa = 0.1$ in $0.1 \lesssim \phi/T$ and that via the CKT prescription. The right panel of Fig. 8 shows the sphaleron rates along the bubble radios for the benchmark scenario in the right panel of Fig. schematicBG. We calculated the BAU using the WKB method. There are two schemes, which are the FH scheme proposed in Ref. [25, 26] and the CK scheme suggested recently in Ref. [27]. We performed

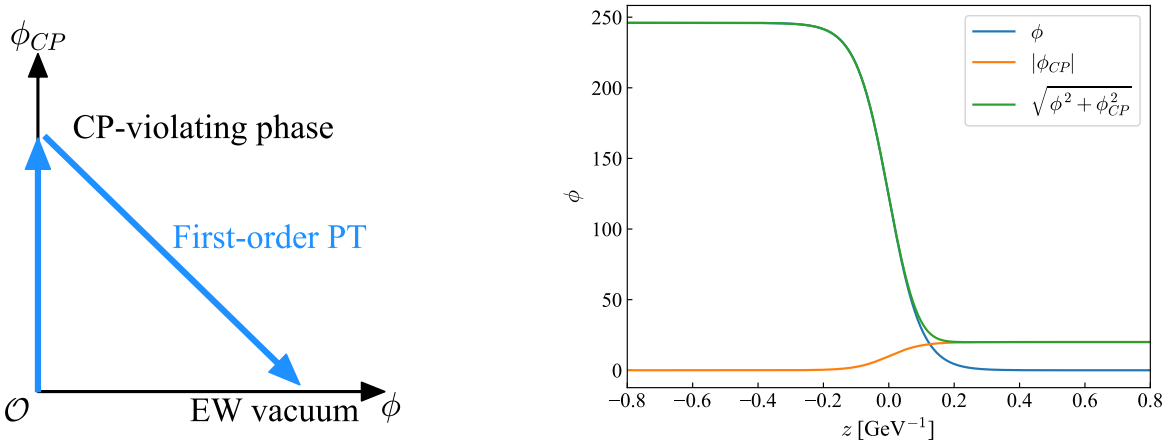

Figure 7 Left: Schematic picture of the multi-step PT for the BAU. Right: Bubble profile of the scalar field values in benchmark scenario.

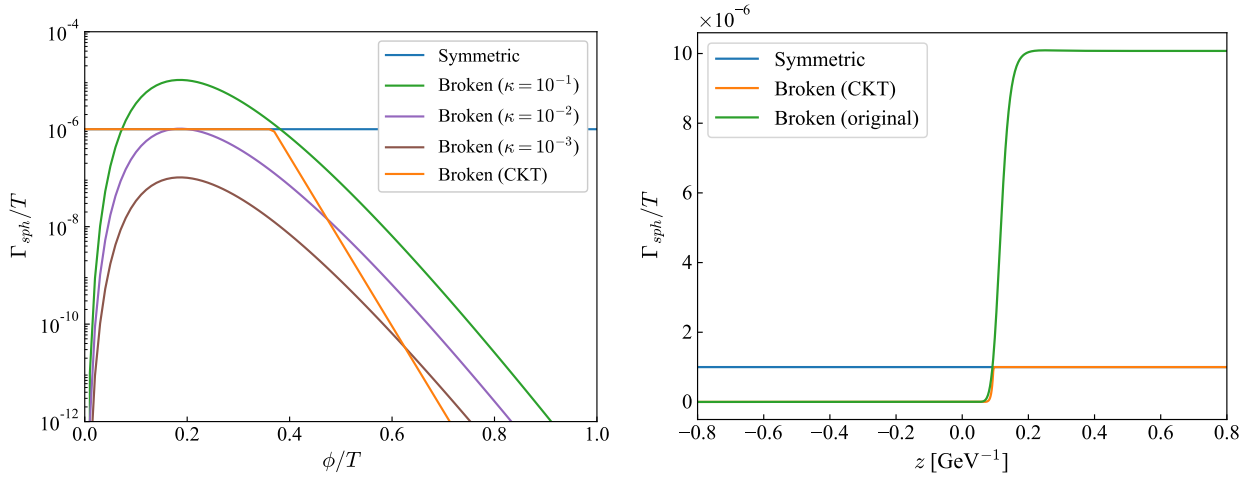

Figure 8 Left: Sphaleron rates $\Gamma_{\rm sph}/T$ as the function of ϕ/T. Right: Sphaleron rates along the bubble radios for the benchmark scenario.

both schemes to verify our results. Fig. 9 shows values of the integrand I, which is defined by $\eta_B \equiv (n_B - n_{\bar{B}})/s = \int_0^\infty dz\ I(z)$ with entropy density s, along the bubble ratio in the FH (left) and the CK (right) scheme. We can see that similar behaviors are obtained in both cases. The difference between the two schemes in Fig. 9 is consistent with the result in Ref. [27]. The green lines are given with the sphaleron rate in the broken phase with $\kappa = 0.1$. Because the rate exceeds that in the symmetric phase as in the right panel of Fig. 8, the integrand enhances outside of the bubble more than the other two plots. Fig. 10 represents produced number density of the BAU via the multi-step PTs in the ϕ vs. ϕ_{CP} planes calculated via the FH (left) and the CK (right) scheme. The upper panels represent the result from the CKT prescription and the lower panels from the sphaleron rate in the broken phase. The color in each point indicates the produced baryon number by the second step PT which occurs from the point to the EW vacuum. The black dotted line shows the upper and lower bound for the BAU based on the Big-Bang nucleosynthesis as $\eta_B = (8.2\text{–}9.2)\times 10^{-11}$ [1]. Hence, the region between the two dotted lines can reproduce the observed BAU. We can see all cases in Fig. 10 can explain the BAU. The differences between the upper and lower panels are the maximum order of the BAU and its points in the ϕ vs. ϕ_{CP} planes. In the lower panels, which use the sphaleron rate in the broken phase, the produced BAU maximizes around $(\phi, \phi_{CP}) = (0, 20\ \text{GeV})$. It is because the rate and

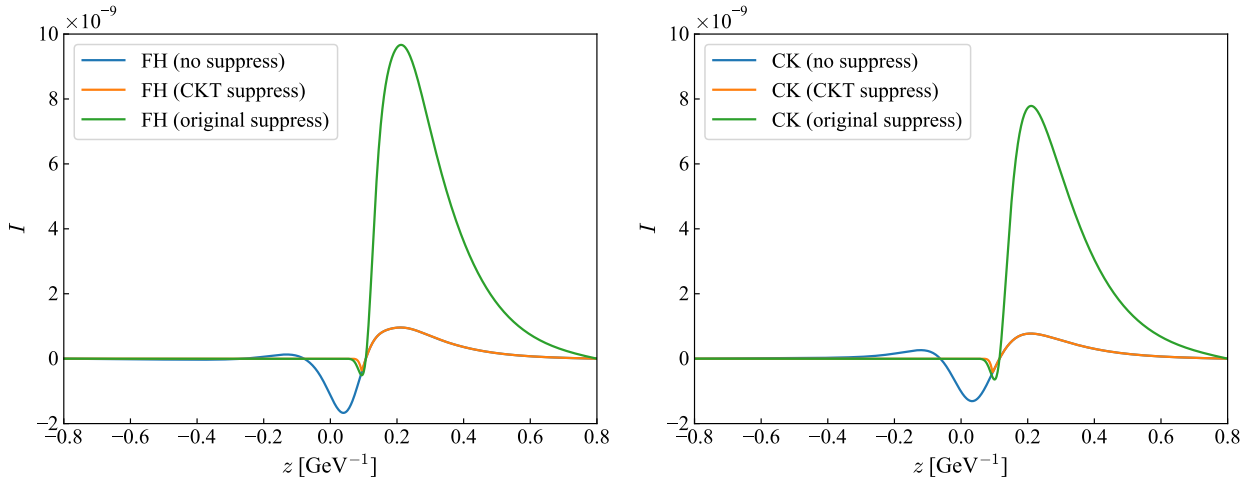

Figure 9 Values of the integrand I ($\eta_B = \int_0^\infty dz\ I(z)$) along the bubble ratio in the FH (left) and the CK (right) scheme.

the change of complex phase in the top mass become the largest at the point. From the above, we consider the simplified scenario. In the dissertation, we discussed specific models which can achieve the BAU via the multi-step PTs. We took the CP-violating 2HDM and the inert 2HDM with higher dimensional operators as examples. Especially the inert 2HDM case was studied in Ref. [28] and denied the possibility of the BAU by performing a simplified calculation. Ref. [28] indicates the sphaleron rate before the second PT is always much more suppressed than that in the symmetric phase. However, we perform a more precise calculation and found the parameter sets where the multi-step PTs occur without the suppression of the sphaleron rate. Hence, our EWBG scenario via the multi-step PT could be realized.

References

[1] Particle Data Group Collaboration, P. A. Zyla et. al., PTEP **2020** (2020), no. 8 083C01.

[2] Planck Collaboration, N. Aghanim et. al., Astron. Astrophys. **641** (2020) A6 [1807.06209]. [Erratum: Astron.Astrophys. 652, C4 (2021)].

[3] C. L. Cowan, F. Reines, F. B. Harrison, H. W. Kruse and A. D. McGuire, Science **124** (1956) 103–104.

[4] Super-Kamiokande Collaboration, Y. Fukuda et. al., Phys. Rev. Lett. **81** (1998) 1562–1567 [hep-ex/9807003].

[5] A. Sakharov Sov. Phys. Usp. **34** (1991), no. 5 392–393.

[6] M. Kobayashi and T. Maskawa, Prog. Theor. Phys. **49** (1973) 652–657.

[7] ATLAS Collaboration, G. Aad et. al., Phys. Lett. B **716** (2012) 1–29 [1207.7214].

[8] CMS Collaboration, S. Chatrchyan et. al., Phys. Lett. B **716** (2012) 30–61 [1207.7235].

[9] M. D'Onofrio, K. Rummukainen and A. Tranberg, Phys. Rev. Lett. **113** (2014), no. 14 141602 [1404.3565].

[10] D. Land and E. D. Carlson, Phys. Lett. B **292** (1992) 107–112 [hep-ph/9208227].

[11] M. Aoki, T. Komatsu and H. Shibuya, PTEP **2022** (2022), no. 6 063B05 [2106.03439].

[12] G. Dorsch, S. Huber and J. No, JHEP **10** (2013) 029 [1305.6610].

[13] M. Cepeda et. al., CERN Yellow Rep. Monogr. **7** (2019) 221–584 [1902.00134].

[14] K. Fujii et. al., 1506.05992.

[15] C. Caprini et. al., JCAP **03** (2020) 024 [1910.13125].

[16] S. Kawamura et. al., Class. Quant. Grav. **28** (2011) 094011.

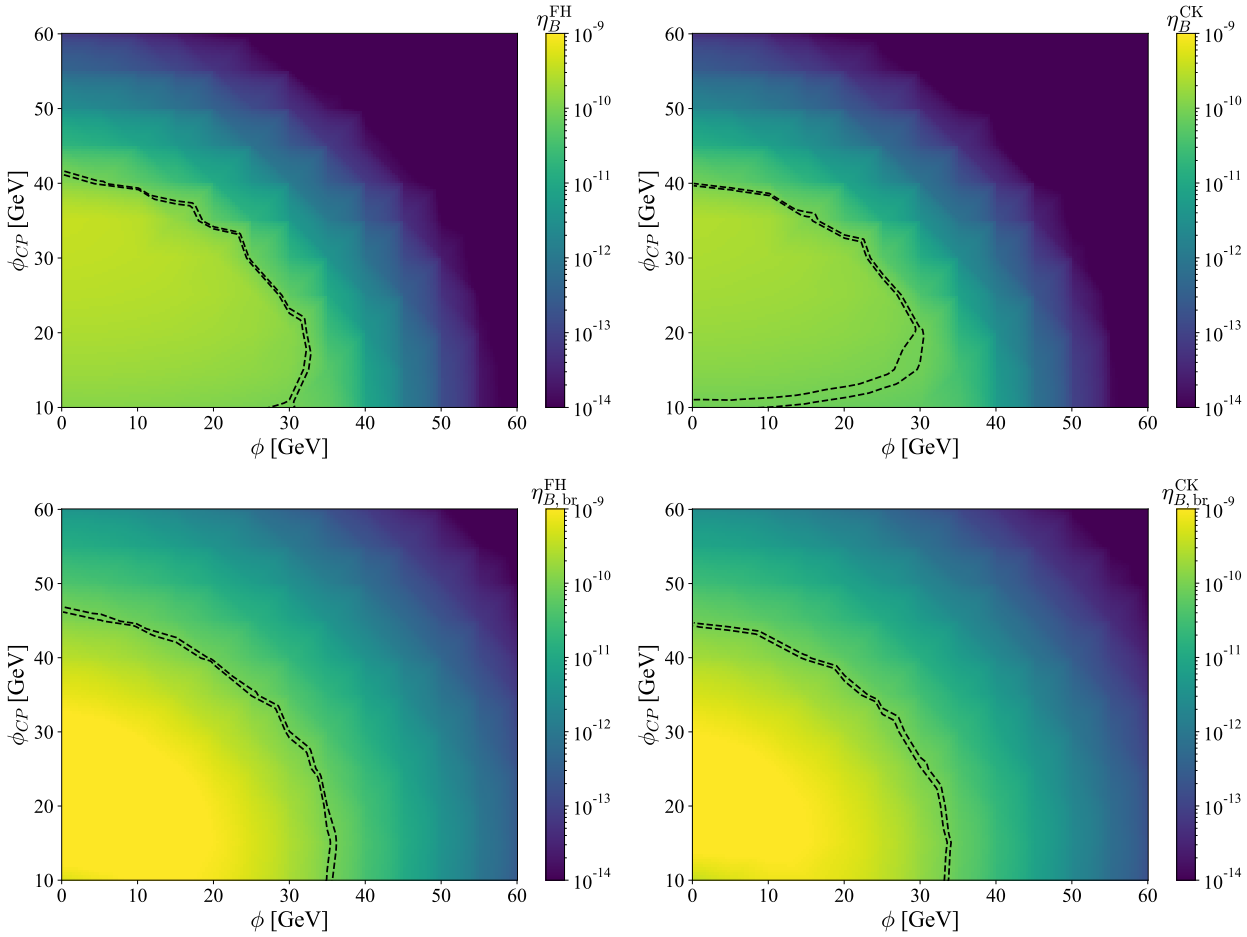

Figure 10 Produced number density of the BAU via the multi-step PTs in the ϕ vs. ϕ_{CP} planes calculated via the FH (left) and the CK (right) scheme. The upper panels represent the result from the CKT prescription and the lower panels from the sphaleron rate in the broken phase.

[17] V. Corbin and N. J. Cornish, Class. Quant. Grav. **23** (2006) 2435–2446 [gr-qc/0512039].

[18] H. Kudoh, A. Taruya, T. Hiramatsu and Y. Himemoto, Phys. Rev. D **73** (2006) 064006 [gr-qc/0511145].

[19] W.-H. Ruan, Z.-K. Guo, R.-G. Cai and Y.-Z. Zhang, Int. J. Mod. Phys. A **35** (2020), no. 17 2050075 [1807.09495].

[20] X.-C. Hu, X.-H. Li, Y. Wang, W.-F. Feng, M.-Y. Zhou, Y.-M. Hu, S.-C. Hu, J.-W. Mei and C.-G. Shao, Class. Quant. Grav. **35** (2018), no. 9 095008 [1803.03368].

[21] H. Shibuya and T. Toma, JHEP **11** (2022) 064 [2207.14662].

[22] E. Ma Phys. Rev. D **73** (2006) 077301 [hep-ph/0601225].

[23] J. M. Cline, K. Kainulainen and M. Trott, JHEP **11** (2011) 089 [1107.3559].

[24] P. B. Arnold and L. D. McLerran, Phys. Rev. D **36** (1987) 581.

[25] L. Fromme and S. J. Huber, JHEP **03** (2007) 049 [hep-ph/0604159].

[26] L. Fromme, S. J. Huber and M. Seniuch, JHEP **11** (2006) 038 [hep-ph/0605242].

[27] J. M. Cline and K. Kainulainen, Phys. Rev. D **101** (2020), no. 6 063525 [2001.00568].

[28] A. Hammerschmitt, J. Kripfganz and M. Schmidt, Z. Phys. C **64** (1994) 105–110 [hep-ph/9404272].

令和 5 年 1月 27 日

学位論文審査報告書（甲）

1．学位論文題目（外国語の場合は和訳を付けること。）

電弱スケールにおける複数段階相転移

2．論文提出者 (1) 所　　属　　数物科学　　専攻

(2) 氏（ふり）　名（がな）　　澁谷（しぶや）　紘人（ひろと）

3．審査結果の要旨（600～650 字）

宇宙は 100 GeV 程度の電弱スケールで相転移(電弱相転移)を起こしている。素粒子の標準模型では、電弱相転移はクロスオーバー転移であることが知られているが、新たなスカラー場を含む拡張模型では一次相転移となる可能性があり、その場合には、なぜ我々の宇宙には反物質が存在しないのか？という物質-反物質非対称性の問題を解決できる可能性が考えられる。さらに、一次相転移で生成された重力波が、将来の宇宙重力波望遠鏡で観測される可能性も期待できる。

澁谷紘人氏は、２つのヒッグス二重項を持つ Two Higgs Doublet 模型(2HDM)では、新たな可能性として、一次相転移を含む複数段階の電弱相転移が起こり得ることに着目し、電荷-パリティ対称性が保存された 2HDM のポテンシャル解析を行い、複数段階相転移の様子を明らかにした。特に、一次相転移を含む複数段階相転移は新ヒッグス粒子の質量差が大きい場合に起こりやすいなど、いくつかの特徴を見出した。また、一次相転移が二回起こる場合には、２つのピークをもつ重力波スペクトルが得られる可能性があり、それが観測出来れば複数段階相転移の有力な証拠となる。澁谷氏は、二段階相転移が起こる場合を精査し、将来の宇宙重力波望遠鏡で検証可能な重力波スペクトルを予言するベンチマークシナリオを示した。

本論文は、２HDM の広いパラメーター領域において、複数段階相転移の実現可能性を初めて明らかにしたものである。レビュー部分や暗黒物質と関連した議論についても適切に記述されており、博士論文に値すると判断した。

4．審査結果　(1) 判　　定（いずれかに○印）　(合　格)　・　不合格

(2) 授与学位　　博　士（　理学　）